Available online at www.sciencedirect.com
ScienceDirect
Journal of Colloid and Interface Science 312 (2007) 481–488
JOURNAL OF Colloid and Interface Science
www.elsevier.com/locate/jcis

Shear-induced structures formed during thixotropic loops in dilute worm-micelle solutions

Jorge Delgado, Rolando Castillo *

Instituto de Física, Universidad Nacional Autónoma de México, P.O. Box 20-364, México D.F. 01000, Mexico

Received 2 December 2006; accepted 11 March 2007

Available online 15 March 2007

Abstract

The shear stress response of the system CTAB/NaSal/water is studied using strain thixotropic loops in the low concentration regime and [NaSal]/[CTAB] = 1. Stress response during up-shear curves depends on the ramping rate. However, stress response during down-shear curves collapses in one curve, no matter the rate used during the ramping down process; it does not depend on the history of the system. In the process of ramping up during the thixotropic loops, the system forms shear-induced structures. We were able to observe them through the scattered light produced by those structures, when the fluid is under shear in the gap of a transparent Couette cell. During the ramping down, the shear-induced structures survive until the shear rate vanishes. Models that describe the form of the up-shear and down-shear curves were presented, as well as, how thixotropic loops can give information about this kind of systems. In particular, for down-shear curves, we can define a decay shear rate constant that follows an Arrhenius temperature dependence.

Keywords: Thixotropic loops; Wormlike micelle; Shear-induced structures; CTAB/salicylate

1. Introduction

Certain surfactant molecules in liquid solution are known to spontaneously self-assemble into cylindrical micelles. Cylindrical micelles in water are usually made of cationic surfactants and of anionic benzyl hydrophobic moieties. In equilibrium and at low surfactant concentration, micelles in the system hexadecyltrimethylammonium bromide (CTAB)/sodium salicylate (NaSal)/water have a radius of ∼2 nm [1], a persistence length of ∼38 nm [1], and micelle contour lengths of ∼10–40 times the persistence length, depending on $R =$ [NaSal]/[CTAB] [1]. These cylindrical micelles [2–5] interact electrostatically among them. Addition of salts in these solutions results in screening the electrostatic micelle interaction and in aggregate growth [1]. These micelles (wormlike) make the fluid where they are embedded to present a strong nonlinear response under imposed flow fields. In the low-concentration micellar regime (<10 mM), wormlike micellar solutions show intriguing properties like shear thickening and rheopexy. Although, quantitative features change from one system to another, wormlike micellar solutions have many characteristics in common. Curves of apparent viscosity vs shear rate, when shear rate is imposed, present shear thickening above a critical shear rate $\dot{\gamma}_c$. After reaching a maximum, where apparent viscosity jumps up by a factor of 20–30, the system shear thins at higher shear rates; before this $\dot{\gamma}_c$ the system is Newtonian or slightly thinning [6,7]. $\dot{\gamma}_c$ increases with concentration as a power law and presents an Arrhenius temperature dependence [2,4–6], i.e., $\dot{\gamma}_c(\phi, T) \sim \phi^{\alpha} \exp[-E/k_B T]$, where E is an activation energy and ϕ is the surfactant concentration. After a sudden application of a constant shear rate larger than $\dot{\gamma}_c$, there is an induction period, τ_{ind}, where shear stress begins to increase sharply up to a steady-flow plateau; $\tau_{ind} \sim 1/\dot{\gamma}_c$ [8]. The higher the temperature the longer the induction period [8]; shear thickening also decreases with temperature [2]. After the induction period, the stationary stress reached at the steady-flow plateau fluctuates appreciably as time elapses (10–50%) [6,8]. Cylindrical micellar solutions that present electrostatic interactions are strongly flow history dependent [8], so specific protocols have been developed to study them [10,11]. It has been

* Corresponding author.
E-mail address: rolandoc@fisica.unam.mx (R. Castillo).

0021-9797/$ – see front matter
doi:10.1016/j.jcis.2007.03.010

noticed by stress relaxation that a major portion of the stress relaxes rapidly upon turning off the flow, but a small stress persists for a long time [12]. Also, these solutions present flow birefringence. The development of a highly aligned phase approximately coincides with the shear thickening transition [3]. For a given shear rate, both the steady-state shear stress and the steady-state flow birefringence, decrease with added salt. As salt concentration increases τ_{ind} and $\dot{\gamma}_c$ increase, and the relaxation time decreases [12]. These results have been interpreted as a consequence of an increase in micelle contour length and micelle lifetime [3]. It has been suggested that micelle aggregation occurs already at shear rates smaller than $\dot{\gamma}_c$, and that the shear thickening occurs once the mean size of the aggregates has reached some critical value [13]. Small-angle neutron scattering (SANS) also shows that structures induced by shear remain long time after the cessation of the shear [14]. However, if the shear rate is removed during the induction period, the stress vanishes to zero instantaneously [8]. SANS studies strongly suggest that the increase in viscosity observed above $\dot{\gamma}_c$ is associated with a shear-induced growth of the micellar aggregates [14]. From SANS scattering data under shear [2], it was established a correlation between flow and structure. In the thickening region, observations are attributable to the superposition of two coexisting states, one made of a viscoelastic entangled sheared network and another made of short aggregates purely viscous. At higher $\dot{\gamma}$, the former state dominates and an increasing orientational order results in shear thinning. Light scattering experiments [6,15,16] suggest that the shear thickening effect is a shear-induced gelation followed by a fracture of the gel [13]. The sheared–induced gel-like and oriented phase is made of shear-induced structures (SIS) forming large fluctuating domains that are coexisting with a homogeneous fluid phase containing small rod-like micelles. In particular, using small angle light scattering, it was clear the emergence of long rod-like structures along the flow direction, which start their formation at the shear-thickening transition, where stress also starts to grow up [6]. No appreciable spacing correlation between them was observed along the flow direction, and light scattering experiments indicate that the rod-like structures may be long micellar bundles forming entangling fibers [6].

From the theoretical point of view, the dynamics of self-assembly of rigid rod-like micelles under both shear and elongational flow has been studied neglecting long-range forces among micelles [17,18]. In elongational flow, at some critical flow rate, a gelation transition was predicted to a phase of extremely long rods, which are aligned with the flow axis. For the case of shear flow it is expected that inter-micelle interactions, even if small, could induce a similar transition. Kinetic theory suggests a flow-induced first-order gelation due to the increase in rodlike micelle size as a consequence of the shear [19].

The aim of this paper is to present for the first time a convenient flow history to study formation and dismantling of SIS in the system CTAB/NaSal/water, in the low concentration regime (0.2–3 mM) at $R = 1$. Stress response measurements and direct SIS observation using light scattering during strain thixotropic loops were carried out. This experimental method allowed us to split the shear stress response during up shear thixotropic curves in two contributions, one from SIS formation and another from the supporting unstructured fluid. A population growth model, supported by the light scattering experiments, captures SIS formation. In addition, we show that thixotropic down-shear curves are independent of the flow history. Again, direct observation of SIS allow us to propose a viscoelastic model that captures SIS dismantling. This model provides us a way to define a decay shear rate constant that follows an Arrhenius behavior with temperature.

2. Experimental methods

2.1. Materials

CTAB, ⩾99%, from Fluka (Switzerland) and NaSal, ⩾99.5%, from Sigma-Aldrich (USA) were used as received. Micellar solutions were prepared by weight. Measurements were made at least three days after the solution preparation to allow them to reach equilibrium [20]. To assure that the solution was above the critical micelle concentration (CMC), we determined it. CMC = 0.093 mM in CTAB for $R = 1$, at 20 °C (details in the Supporting material).

2.2. Methods

Rheometric measurements were made with a modified cone–plate rheometer (RV-III + Brookfield, USA), a Bohlin Gemini HRnano (Malvern Instruments, UK), and a homemade transparent Couette rheometer. The cone–plate rheometer controls shear rate and was modified to include in the plate a glass window for allowing fluid visualization (diagram in Supporting material). Most of the rheometric measurements were done using the same cone–plate geometry (1.565°, 48 mm diameter). When other geometries are used, the shape of flow curves is the same; although, the actual stress response values are different. A study involving different geometries has been made by Hu et al. [13,21]. The transparent Couette rheometer (Fig. 1) is made

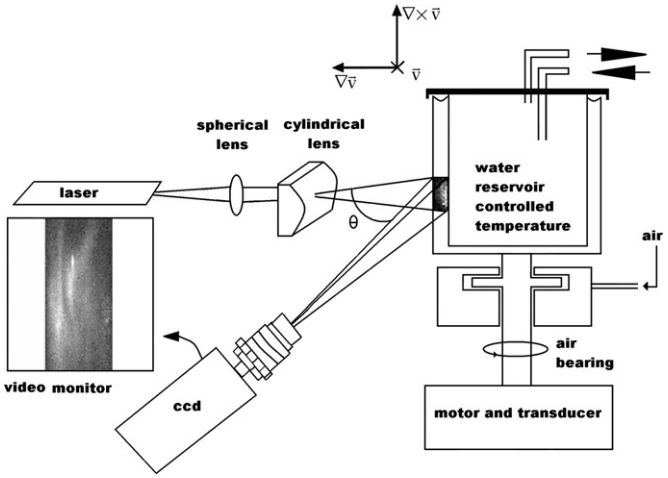

Fig. 1. Transparent Couette rheometer formed by two concentric quartz cylinders. The external cylinder rotates over air bearings. The fluid in the gap (2.5 mm) is visualized with the aid of a CCD camera and a zoom lens focused at a sheet of light made with a Ne–He laser beam and a couple of lenses.

of two concentric quartz cylinders (50 mm height). The inner cylinder (O.D. 75 mm) is fixed and filled with water coming from a thermal regulated circulatory bath for thermal control. The external cylinder (O.D. 85 mm) rotates over air bearings; both shear and stress modes can be used with the aid of a dc-motor (Maxon Motors, Germany). The gap between cylinders is 2.5 mm wide. A section of the gap with the fluid can be visualized using a zoom lens combination focused at a sheet of light made with a Ne–He laser beam (Coherent Inc., USA) and a combination of spherical and cylindrical lenses. The zoom lens is mounted on a video camera (Hamamatzu Vidicon, Japan).

3. Results and discussion

3.1. Shear stress growth and decay functions in thixotropic loops

In a thixotropic loop (TL) the shear rate is first ramped up (up-shear curve) to some maximum value $\dot{\gamma}^{M}$ and then it is ramped down (down-shear curve) at the same rate to zero. As will be shown below, the use of TLs creates a convenient flow history to study wormlike micellar solutions. At the beginning of the up-shear process, the system lags behind forming SIS and their increment can be followed by the nonlinear increment in the shear stress growth function $\sigma^{+}(t,\dot{\gamma})$. Since, the time to reach a specific $\dot{\gamma}_s$ where SIS can be formed in a TL, is short compared to the slow growing of wormlike micelles and bundles at constant $\dot{\gamma}_s$, where induction times are ∼600 s [6]. We are decoupling the stress response due to SIS formation from that related to the unstructured fluid. On ramping down, the system is also lagging behind, but now dismantling the SIS produced on ramping up. In this case, the non-linear decrease in the shear stress decay function $\sigma^{-}(t,\dot{\gamma})$ probes the maximum amount of SIS for every imposed shear rate.

Fig. 2 shows a typical shear stress growth function $\sigma^{+}(t,\dot{\gamma})$ vs $\dot{\gamma}$ for a dilute micellar solution ([CTAB] = 1 mM, $R = 1$) at 20 °C, where the shear stress response of the solution for an increasing shear rate sweep starting at $\dot{\gamma} = 0$ is observed (shear rate sweep = 0.53 s^{-2}). In this figure, we also included the same kind of measurement for water. For the micellar solution, the first part of the up-shear curve follows a sigmoidal behavior, where the system shear thickens steadily up to a certain point at $\dot{\gamma} \sim 100\ s^{-1}$. After here, the shear stress grows linearly with the shear rate; we will call this region the linear regime. Here, the slope of the flow curve for both the micellar solution and water is the same (0.001 Pa s^{-1}). It looks like as if the stress increment in this linear regime was mainly due to the most abundant component in the system, i.e., water. A sigmoidal logistic function plus a linear term in $\dot{\gamma}$ were used to fit the $\sigma^{+}(t,\dot{\gamma})$ vs $\dot{\gamma}$ curves for the micellar solution and a linear function in $\dot{\gamma}$ for fitting water. The fitting for the micellar solution was excellent; we will come back to this issue below. Taking into account the facts mentioned for the system of interest here in Section 1, the sigmoidal behavior of $\sigma^{+}(t,\dot{\gamma})$ make us suspect that during this stress increment bundles of wormlike micelles are formed, i.e., the SIS [6]. A sample of the micellar fluid was placed in a cone–plate geometry cell with an

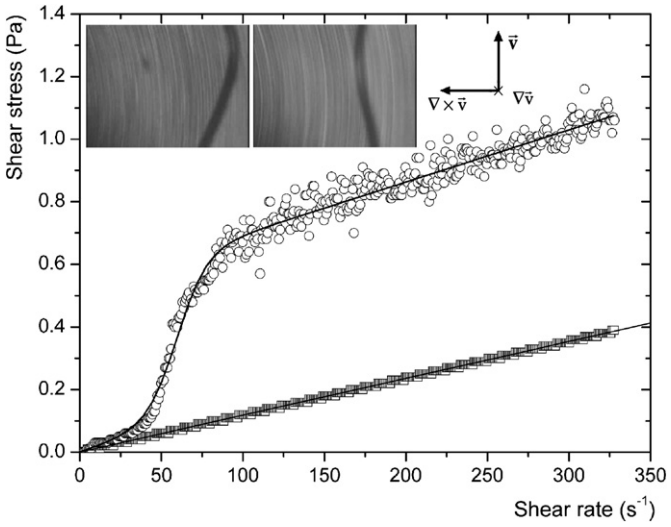

Fig. 2. $\sigma^{+}(t,\dot{\gamma})$ vs $\dot{\gamma}$ for a dilute micellar solution (○) at 20 °C ([CTAB] = 1 mM, $R = 1$) and for water (□), showing the shear stress response for an increasing shear rate sweep (0.53 s^{-2}). Continuous lines are fittings to data; Eq. (2) was used for the micellar solution and a linear fitting for water. Insets: deformed fluid/air interface (dark line: interface; micellar fluid: left; air: right) as observed through the window in the plate of a cone–plate rheometer shown in Fig. 1 in the Supporting material. Images obtained at $\dot{\gamma} = 245\ s^{-1}$ (left) and at $\dot{\gamma} = 286\ s^{-1}$ (right); dimensions: 2.3 × 1.7 mm.

observation window in the plate, to observe the fluid with polarized light while it is sheared (Fig. 1 in the Supporting material). Depending on the sample volume placed in the cell, we can observe the bulk of the fluid or the micellar fluid/air interface (not filling the entire cell). At low shear rates, far below from the linear regime, the micellar fluid presents a circular fluid/air interface as expected for Newtonian fluids (not shown). However, as the shear rate is increased, the fluid/air interface presents an undulated deformation (thick dark line in the inset of Fig. 2) that is not present in water or in Newtonian standard oils at the same shear rates. The amplitude of this deformation increases as the shear rate increases, until the stress reaches the linear regime. Here, the amplitude of the deformation looks constant and the fluid never breaks up; it behaves as an elastic fluid. This undulation is probably responsible for the stress fluctuation in the linear regime that can be observed in Fig. 2 for the micellar fluid. It is important to note that we just report $\sigma(t,\dot{\gamma})$ vs $\dot{\gamma}$ curves when the cell is completely filled.

In Fig. 3, we present typical examples of flow curves $\sigma^{+}(t,\dot{\gamma})$ vs $\dot{\gamma}$ and $\sigma^{-}(t,\dot{\gamma})$ vs $\dot{\gamma}$ in TLs carried out for dilute micellar solutions ([CTAB] = 1 mM, $R = 1$, $T = 20$ °C). Here, up-shear and down-shear curves were obtained in consecutive loops, where the ramping rates go from 0.53 up to 2.64 s^{-2}, with 5 min of waiting time between loops. We included only one down-shear curve for comparison in Fig. 3; all down-shear curves are presented in the inset. In a loop, the up-shear and down-shear curves are different, except in the linear regime where they coincide. The most important feature is that all down-shear curves corresponding to the different shear rate sweeps collapse in just one curve and in general, it does not return to $\sigma^{-}(t,\dot{\gamma}) = 0$ at $\dot{\gamma} = 0$. We checked up with a Newtonian silicon oil standard that the remnant stress was not

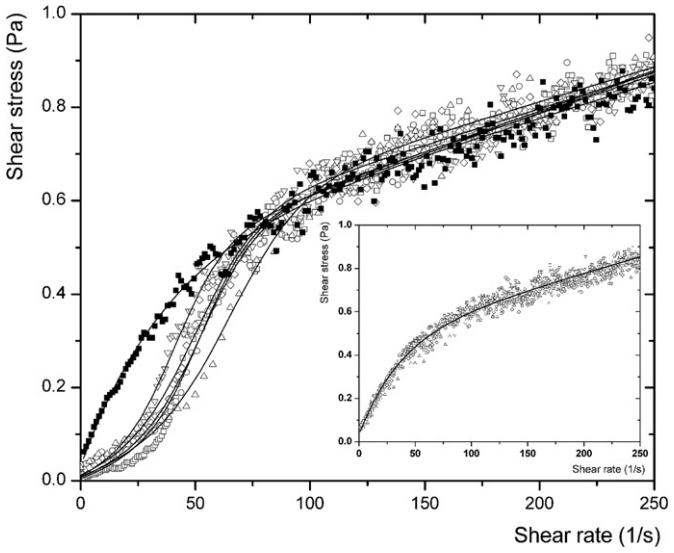

Fig. 3. Curves showing the up-shear curves for consecutive thixotropic loops. Sweep: 0.53 (□), 0.79 (▽), 1.32 (◇), 1. 59 (○), and 2.64 s^{-2} (△) and for one down-shear curve: sweep −0.79 s^{-2} (■). Inset: down-shear curves for all consecutive thixotropic loops presented in the figure. Continuous lines are fittings to data; Eq. (2) was used for up-shear curves and Eq. (6) for down-shear curves.

related to an inertial contribution from the rheometer. The up-shear curves seem to be sigmoidal at low $\dot{\gamma}$ and, in general, as the shear rate sweep increases the sigmoidal part of the up-shear curves moves to high shear rate values. However, this behavior depends in a nontrivial manner on the system history. For instance, the first curve corresponding to a shear rate sweep of 0.53 s^{-2} was obtained after a very long relaxation time (days); it is on the right from the curve corresponding to the second loop ramped up at 0.79 s^{-2}. In all up-shear curves, we reached a noisy linear regime at $\dot{\gamma} \sim 100$–$120\ s^{-1}$, where $\sigma^+(t, \dot{\gamma})$ depends linearly on $\dot{\gamma}$.

3.2. Observation of the shear-induced structures

In Fig. 4, we present images of the light scattered from a dilute solution ([CTAB] = 3 mM, $R = 1$, 20 °C) under shear during a TL, giving a direct evidence of SIS formation. Light is scattered from a sheet of light perpendicular to the flow, which is installed in the gap of a transparent Couette cell filled with the micellar fluid (see Fig. 1). Light scattering reveals fluctuations in the dielectric constant due to fluctuations in density and in the nematic order parameter. The images for the ramping up process are shown in the lower panel of Fig. 4. The scattered light from the fluid is homogeneous along the observation window, from $\dot{\gamma} = 0$ until the system reaches $\dot{\gamma} \sim 50\ s^{-1}$ that corresponds approximately to the beginning of the sigmoidal part of the up-shear curves, as shown in the intermediate panel of Fig. 4; this is a sketch of the shear stress response during a TL. After $\dot{\gamma} \sim 50\ s^{-1}$, we observe the formation of irregular bright and dark stripes. These bright stripes are the SIS [6] and the dark stripes are the unstructured fluid. The bright stripes become brighter and more defined as the fluid reaches the linear regime. Thus, in the up-shear curves of TLs, SIS are formed until shear rate reaches certain level, then they grow as the shear rate increases until the linear regime is reached. In recorded films from the scattering experiments, these stripes look like fluctuating. For an observer perpendicular to the sheet of light, these stripes are neither fully aligned with the flow nor forming stationary structures along the Couette gap. However, they are statistically more aligned in the vertical direction, as if they were part of vertical inhomogeneous thick sheets parallel to the flow and coming to the observer along the flow direction. These vertical sheets separated by the unstructured fluid never form two separated blocks or regions in the fluid, confirming the result of another group controlling $\dot{\gamma}$ [22]. The images during ramping down are shown in the upper panel of Fig. 4. Here, in the linear regime where the down-shear curve starts, we observe deformed and bright stripes (better noticed in recorded films of experiments), but when the shear rate is ramped down they are not as brilliant and well defined as in the linear regime. SIS do not completely disappear during the ramping down and we never found a state where the fluid homogeneously scatters light, except after some relaxing time (a couple of seconds) after the ramping down process has finished. The images of Fig. 4 allow us to understand more clearly why up-shear and down-shear curves in TLs are so different. In the former case, the shear stress growth function probes the delayed formation of SIS, and in the latter case the shear stress decay function describes how the SIS decline as the shear is lowered. A gel phase is not observed in this scattering experiments, so the fluid at high shear rates is formed by a viscous continuous part (water-rich phase) and by viscoelastic discontinuous stripes forming a network made of bundles of wormlike micelles (SIS) [2].

3.3. Models for describing up-shear and down-shear curves

In TLs, if the non-linear shear stress increment during the ramping up reveals the formation of SIS, it is possible to propose a model for explaining the shape of up-shear curves. In $\sigma^+(t, \dot{\gamma})$, it is necessary to recognize that there is a contribution from the solvent, σ_s, and another stress contribution due to SIS; we will call the later as: $\sigma_{SIS} = \sigma^+(t, \dot{\gamma}) - \sigma_s$. This is suggested from the results of Fig. 2, where we observe that there is a contribution for $\sigma^+(t, \dot{\gamma})$ that goes linearly with the shear rate, $\sigma_s \sim c\dot{\gamma}$. Up-shear curves and the evidence of SIS formation suggest that we could describe the shear stress contribution due to SIS as a growing function, similar to those used in population growth, resulting from the growth of the structures induced by shear, with a relative growth rate $k > 0$. Implicitly, we are assuming that σ_{SIS} is a linear function of the amount of SIS formed in the fluid, as suggested by Barentin and Liu [9]. However, it cannot be allowed that the SIS growth could be unconstrained, because of the finite number of surfactant molecules in the system and as a consequence, the number of induced aggregates that can be formed. Thus, the fractional increase in shear stress, due to the contribution of SIS, could be modeled by a population growth equation of the following form:

$$\frac{1}{\sigma_{SIS}} \frac{d\sigma_{SIS}}{d\dot{\gamma}} = k\left[1 - \frac{\sigma_{SIS}}{\sigma_M}\right]. \tag{1}$$

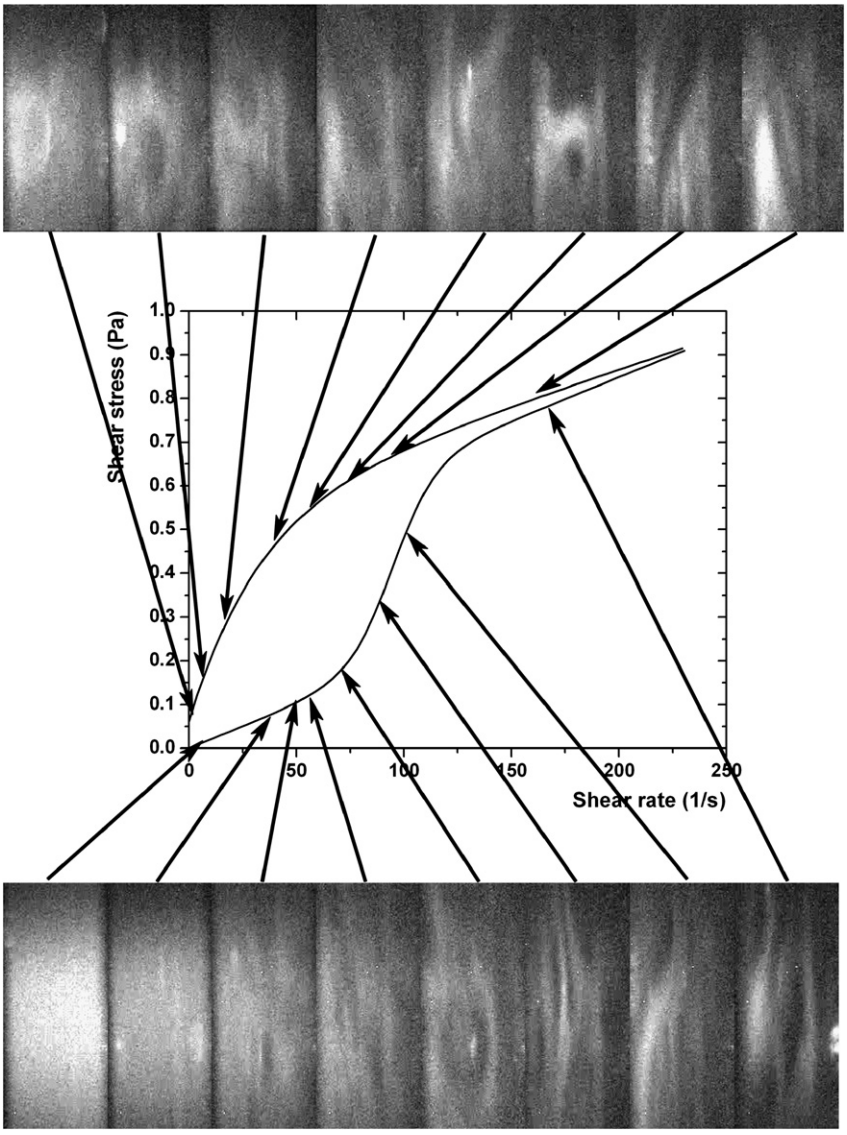

Fig. 4. Images of the light scattered from a sheet of light, perpendicular to the flow direction, installed in the gap of a transparent Couette cell filled with the micellar fluid ([CTAB] = 3 mM, $R = 1$, 20 °C). The images were obtained during a TL developed with a ramp of 0.54 s^{-2}. The images were obtained approximately at the shear rate indicated by arrows. Upper panel: observations on ramping down; medium panel: the shear response during a TL; lower panel: observations on ramping up.

Here, stress growth is constrained due to the term σ_{SIS}/σ_M that prevents shear stress to increase without a limit. σ_M is the maximum stress due to SIS formation, i.e., $\sigma_M = \sigma^+(t, \dot{\gamma}) - \sigma_s$ after the sigmoidal growth in Fig. 2. Equation (1) can be easily integrated and an expression for $\sigma^+(t, \dot{\gamma})$ can be written as:

$$\sigma^+(t, \dot{\gamma}) = \frac{\sigma_M}{1 + [(\sigma_M - \sigma_0)/\sigma_0]e^{-k\dot{\gamma}}} + c\dot{\gamma}, \tag{2}$$

where σ_0 is the σ_{SIS} value for $\dot{\gamma} \sim 0$. We used this function to fit the data for the up-shear curves in Fig. 3, as well as in Fig. 2. Most of the fittings were reasonably well, but in some cases there is a small misfit at the very beginning of the sigmoidal part of the up-shear curves. Probably, the misfit reveals that in some cases our model does not capture another kinetic process in course.

On ramping down in the TLs, the shear stress decay functions, $\sigma^-(t, \dot{\gamma})$, start in the linear regime and below this regime they do not retrace the up-shear curves. In the linear regime, the shear stress response suggests that the total amount of SIS to be formed, due to the amount of available surfactant in the mixture, is already formed [2] (see step strain experiments in the supplementary material). The increase in shear stress response seems to be just due to the solvent contribution. During the down-shear process, there is a stress decline due to SIS dismantling as observed by light scattering as a loss of brightness and definition in the fluctuating stripes. This stress decline, in conjunction with the fading away of the induced structures, seems to be the way in which SIS relax under shear. We can figure out the form of the down-shear curves, if we consider that the fluid is relaxing as a Maxwellian viscoelastic fluid. This is suggested because the fluid in this shearing state is formed by a complex network of wormlike micelle bundles (SIS) in an unstructured fluid, and these bundles must behave as the entangled long con-

tour length micelles at high concentration regimes, where the fluid is Maxwellian [1,2,23]. Therefore, $\sigma^-(t,\dot\gamma)$ must follow the equation:

$$\sigma^- + \tau\dot\sigma^- = \eta\dot\gamma. \tag{3}$$

Here, the time constant is $\tau = \eta/G$, where η is the shear viscosity and G is the elastic modulus. Introducing in Eq. (3) the ramping down condition for $\dot\gamma$:

$$\dot\gamma = \ddot\gamma_0 t + \dot\gamma_M, \tag{4}$$

where $\ddot\gamma_0$ is the imposed constant shear rate sweep ($\ddot\gamma_0 < 0$ for ramping down). The equation governing the form of the down-shear curves is obtained substituting Eq. (4) in Eq. (3):

$$\dot\sigma^- + \frac{\sigma^-}{\tau} = \frac{\eta}{\tau}(\ddot\gamma_0 t + \dot\gamma_M). \tag{5}$$

The solution for Eq. (5) can be easily obtained:

$$\sigma^-(\dot\gamma,t) = -\eta\ddot\gamma_0\tau + \eta\dot\gamma + (\sigma_0 + \eta\ddot\gamma_0\tau)e^{-(\dot\gamma/\ddot\gamma_0\tau)}. \tag{6}$$

We used this function to fit the down-shear curves, with excellent results as can be observed in Fig. 3. This model captures the decrease in $\sigma^-(t,\dot\gamma)$ due to the decline of SIS that reached a maximum population value in the linear regime.

Up-shear and down-shear curves fitting parameters are displayed in Table 1. The parameters related to the slope for the linear regime and for the maximum stress produced by SIS are quite similar, in both up-shear and down-shear curves. As mentioned, the slope parameters for the linear regime are also similar to the slope of the flow curve for water. The time constants, k, related to the growth rate of SIS for all the up-shear curves are quite close; they are in the range of 0.100–0.072 s. The decay shear rate constant $\dot\Gamma_c = \ddot\gamma_0\tau$ that characterizes the decay in down-shear curves is similar for all down-shear curves. The inverse of this quantity, $\dot\Gamma_c^{-1} = 1/\ddot\gamma_0\tau$ fluctuates between 0.021 and 0.031 s, and it must be a characteristic time for SIS decline. Fluctuations in these parameters reflect in some way the fast fluctuations in the stress response functions.

Table 1
Fitting parameters for the models for up-shear and down-shear curves

Fitting parameters for Eq. (2) for up-shear curves with an imposed $\ddot\gamma_0$				
$\ddot\gamma_0$ (s^{-2})	σ_0 (Pa)	σ_M (Pa)	c (Pa s)	k (s)
0.53	0.004	0.442	0.002	0.090
0.79	0.010	0.436	0.002	0.090
1.32	0.012	0.484	0.002	0.072
1.60	0.007	0.457	0.002	0.079
2.64	0.009	0.513	0.001	0.062
0.66	0.115	0.555	0.002	0.095
1.30	0.016	0.577	0.001	0.072
2.72	0	0.488	0.002	0.100

Fitting parameters for Eq. (6) for down-shear curves with an imposed $\ddot\gamma_0$				
$\ddot\gamma_0$ (s^{-2})	$-\eta\ddot\gamma_0\tau$ (Pa)	η (Pa s)	$-(\sigma_0+\eta\ddot\gamma_0\tau)$ (Pa)	$1/\ddot\gamma_0\tau$ (s)
−0.53	0.472	0.002	0.441	0.031
−0.79	0.475	0.001	0.442	0.027
−1.32	0.484	0.001	0.457	0.025
−1.60	0.445	0.002	0.434	0.031
−2.65	0.463	0.001	0.465	0.023
−0.94	0.435	0.002	0.385	0.030
−0.66	0.535	0.002	0.474	0.031
−1.33	0.557	0.001	0.505	0.025
−2.72	0.648	0.001	0.571	0.021

3.4. Temperature dependence of thixotropic loops and $\dot\Gamma_c$

Temperature modifies the shear stress response in TLs as observed in Fig. 5 for down-shear curves. TLs were performed at a constant sweep rate of $\pm 0.92\ s^{-2}$ and with waiting times between loops of at least 15 min after reaching the selected temperatures. Down-shear curves show a transition shoulder from high $\dot\gamma$ values (linear regime) to lower ones, and this shoulder is less pronounced as temperature increases. These curves reveal that the maximum shear stress reached by the solutions decreases with temperature. Therefore, the lower the temperature the larger amount of induced structures. In up-shear curves, as temperature increases, the sigmoidal stress increment moves to high $\dot\gamma$ values and the maximum stress produced by SIS decreases (see Supporting material).

As described in Section 1, at constant deformation rate and above a critical shear rate $\dot\gamma_c$, initial stress or viscosity increase after some induction time [2,6–9]. But, on approaching $\dot\gamma_c$, induction times are very large and stress fluctuations also grow. Then, it is difficult to get a reliable value for $\dot\gamma_c$ [10–12]. As shown above, down-shear curves in TLs do not depend on the flow history of the sample. Any ramping down curve always produces the same curve. Therefore, down-shear curves are characteristic curves for the system and the parameter $\dot\Gamma_c$ obtained from the fitting of experimental curves is also a characteristic decay parameter for stress decline, related to the process of dismantling the bundles. This decay parameter $\dot\Gamma_c$ also follows an Arrhenius-type temperature dependence with a form

$$\dot\Gamma_c = Ae^{(-\Delta E_a/k_B T)},$$

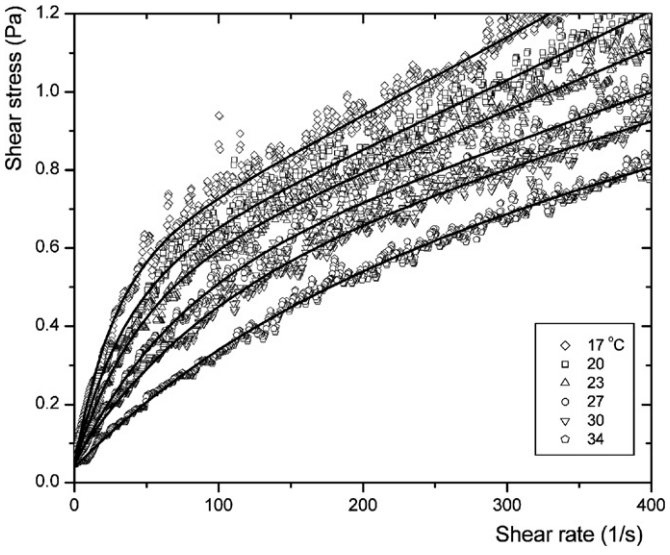

Fig. 5. Behavior of the down-shear curves for the thixotropic loops as temperature is modified. Temperatures: 17 (◇), 20 (□), 23 (△), 27 (○), 30 (▽) and 34 °C (⬠). Continuous lines are fittings to data using Eq. (6).

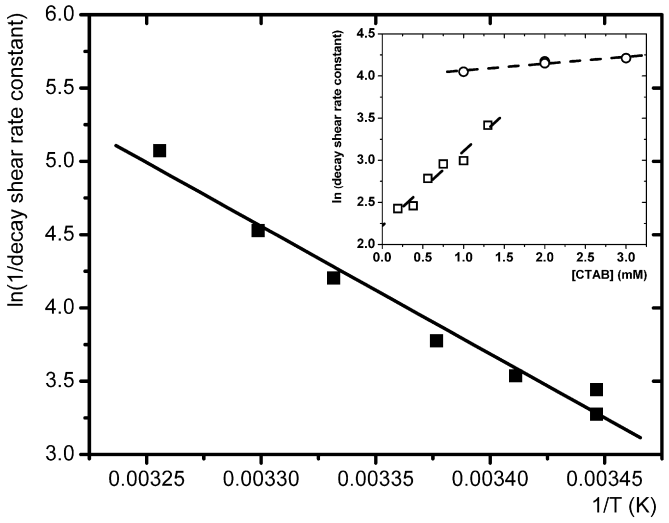

Fig. 6. Arrhenius-type temperature dependence for $\dot{\Gamma}_c = \ddot{\gamma}_0\tau$. $\dot{\Gamma}_c$ values were obtained from fitting Eq. (6) to the experimental results presented in Fig. 5. Inset: $\dot{\Gamma}_c$ as a function of surfactant concentration at $R = 1$ and 20 °C. Measurements were done using a cone–plate geometry with cones with two different angles: 3.000° (□) and 1.565° (○).

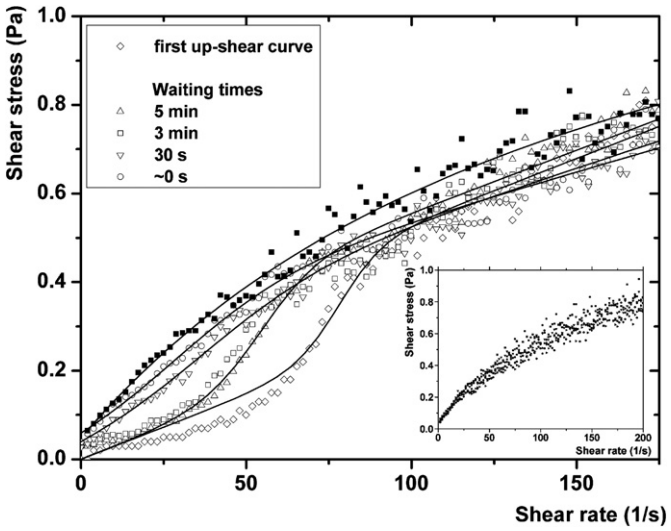

Fig. 7. Thixotropic loops (ramping sweep 1.13 s^{-2}) where waiting times between consecutive loops are reduced. As the waiting time is reduced the up-shear curves (open symbols) are closer to the down-shear curves (■). Inset, all the down-shear curves corresponding to the thixotropic curves presented in the figure. Lines are fitting according to Eqs. (2) (up-shear curves) and (6) (down-shear curve).

as it can be observed in Fig. 6, where A is a concentration dependent pre-exponential factor, ΔE_a is an activation energy, and k_B is the Boltzmann constant. From the slope of the curve in Fig. 6, the activation energy can be estimated, $\Delta E_a \sim 30 k_B T$, which is close to the value of 21.5 $k_B T$ obtained by Hu et al. [8] for the same system. In addition, $\dot{\Gamma}_c$ increases logarithmically with ϕ in agreement with the behavior of $\dot{\gamma}_c$ for CTAT [4]. For the same system of interest here, other authors have found that $\dot{\gamma}_c$ decreases linearly with concentration at $R = 0.24$ [20]. $\dot{\Gamma}_c$ plays a similar role as $\dot{\gamma}_c$ that characterizes the shear stress increment after some induction time [2,7–9] but, in our case $\dot{\Gamma}_c$ characterizes the stress decline, with the additional feature that it does not depend on the shear history.

A point to discuss now is related to the question: Once the TL is over: How long do SIS subsist? A partial answer has been given through the characteristic time $\dot{\Gamma}_c^{-1} = 1/\ddot{\gamma}_0\tau \sim$ 0.02–0.03 s. This characteristic time gives us an estimate about the time after which the fluid will follow an up-shear curve different from the down-shear curve, if the TL is restarted. This can be confirmed, making successive TLs where the waiting times between TL are reduced, i.e., SIS are not allowed to be completely dismantled. In Fig. 7, we present successive TLs using the same ramping sweep, but with different waiting times between them. As it can be observed, as the waiting time is reduced up-shear curves are closer to the down-shear curve. For the case of immediately re-start, the waiting time is close to zero, both curves almost coincide (time needed for the rheometer to start again). This waiting time is the closest value to the characteristic time $1/\ddot{\gamma}_0\tau$ for stress decline given in Table 1 that we can reach. (More characteristic features for down shear curves can be seen in the Supporting material). In Fig. 7, we can also observe that SIS can subsist several minutes (∼3–5 min) after a TL is over, because the up-shear curves take this time to be far from the down-shear curve.

3.5. Final remarks

The new evidence shown here agrees with the emerging image for the fluid behavior given in Section 1. During the ramping up, along the sigmoidal curve SIS start to grow. The flow field tends to align the rod micelles existing in the solution and the flow field enhances the end-to-end rate of fusion of rod micelles increasing their average micellar length. This global alignment triggers the next event, the electrostatic interaction among wormlike micelles. When they are aligned, the bad charge distribution on the wormlike micelle surface induces an attractive force. The attractive force overwhelms the repulsive one, due to multipolar electrostatic interactions [9,14] and leads to the formation of bundles of micelles (SIS), which start to interact among them and to be interconnected along the fluid where they are embedded, forming a long 3D network. When the linear regime is reached, an upper limit amount of SIS has been reached. In this regime, all momentum transfer due to shearing is dissipated mainly by the unstructured fluid; here the fluid is apparently a Maxwellian one. During the ramping down, SIS decline because the structures forming them, bundles of wormlike micelles, dismantle. Now, micelles forming bundles are allowed to lose their alignment due to Brownian motion. As the alignment is lost, the net repulsive force makes the micelles to fall apart. As a consequence, most of the bundles are dismantled and the peculiar rheological behavior fades away. However, the efficiency for destroying these induced structures certainly decreases as the size of the aggregates is larger. In the interior of one bundle, the exchange of surfactant molecules is likely to occur mostly between the neighboring micelles forming the bundle, so it should not really contribute to the bundle dissolution. In addition, when a micelle belonging to a bundle breaks, it cannot easily diffuse toward the bulk of the solution; actually there must be a high possibility of a local recombina-

tion. This diffusive mechanism will work just at the borders of the bundles; therefore, disassembling would not be necessarily a rapid process [6,9,14]. This could explain why we observe in general a small remnant shear stress when $\dot{\gamma} = 0$ is reached on ramping down the system. However, to reach thermodynamic equilibrium, the system takes a much longer time.

4. Conclusions

We have obtained the shear stress response for a micellar solution (CTAB/NaSal/water) in the dilute regime during TLs, combined with observations of SIS using light scattering under shear. With this new experimental method the stress response due to SIS formation or decline can be decoupled from the response of the unstructured fluid and can be followed by the nonlinear change of the shear stress. Up-shear curves depend on the ramping rate and the system forms SIS as in a growth process. During down-shear curves, stress response shows SIS dismantling. Unexpectedly, down-shear curves collapse in just one curve, so they do not depend on the history of the system. As far as we know, this is the first time this behavior is observed. A viscoelastic model for SIS dismantling under shear allows us to define a decay shear rate constant that increases logarithmically with surfactant concentration and follows an Arrhenius temperature dependence.

Acknowledgments

The support from SEP-CONACYT (46778) and DGAPA-UNAM (IN110505) is gratefully acknowledged. J. Delgado thanks CONACYT (166853) and DGEP-UNAM for financial support. We thank to C. Garza and S. Ramos for their technical support and critical discussions with Ivan Santamaria.

Supporting material

The online version of this paper has a supporting material. Please visit DOI:10.1016/j.jcis.2007.03.010.

References

[1] J.F. Berret, in: R.G. Weiss, P. Terech (Eds.), Molecular Gels, in: Materials with Self-Assembled Fibrillar Networks, Springer, The Netherlands, 2006, p. 663.
[2] J.-F. Berret, R. Gámez-Corrales, J. Oberdisse, L.M. Walker, P. Lindner, Europhys. Lett. 41 (1998) 677.
[3] V. Croce, T. Cosgrove, G. Maitland, T. Hughes, G. Karlsson, Langmuir 19 (2003) 8536.
[4] U.R.K. Rao, C. Manohar, B.S. Valaulikar, R.M. Iyer, J. Phys. Chem. 91 (1987) 3286.
[5] J.-F. Berret, R. Gámez-Corrales, Y. Séréro, F. Molino, P. Lindner, Europhys. Lett. 54 (2001) 605.
[6] C. Liu, D.J. Pine, Phys. Rev. Lett. 77 (1996) 2121.
[7] R. Gámez-Corrales, J.F. Berret, L.M. Walter, J. Oberdisse, Langmuir 15 (1999) 6755.
[8] Y. Hu, S.Q. Wang, A.M. Jamieson, J. Rheol. 37 (1993) 531.
[9] C. Barentin, A.J. Liu, Europhys. Lett. 55 (2001) 432.
[10] J.-F. Berret, R. Gámez-Corrales, S. Lerouge, J.-P. Decruppe, Eur. Phys. J. E 2 (2000) 343.
[11] P. Ballesta, S. Manneville, Europhys. Lett. 76 (2006) 429.
[12] Y. Hu, C.V. Rajaram, S.Q. Wang, A.M. Jamieson, Langmuir 10 (1994) 80.
[13] H. Hu, R.G. Larson, J.J. Magda, J. Rheol. 46 (2002) 1001.
[14] R. Oda, V. Weber, P. Lindner, D.J. Pine, E. Mendes, F. Schosseler, Langmuir 16 (2000) 4859.
[15] Y.T. Hu, P. Boltenhagen, D.J. Pine, J. Rheol. 42 (1998) 1185.
[16] Y.T. Hu, P. Boltenhagen, E. Matthys, D.J. Pine, J. Rheol. 42 (1998) 1209.
[17] M.E. Cates, M.S. Turner, Europhys. Lett. 11 (1990) 681.
[18] M.S. Turner, M.E. Cates, J. Phys. Condens. Matter 4 (1992) 3719.
[19] R. Bruinsma, W.M. Gelbart, A. Ben-Shaul, J. Chem. Phys. 96 (1992) 7710.
[20] R. Cressely, V. Hartmann, Eur. Phys. J. B 6 (1998) 57.
[21] J.Y. Lee, J.J. Magda, H. Hu, R.G. Larson, J. Rheol. 46 (2002) 195.
[22] P. Boltenhagen, Y. Hu, E.F. Matthys, D.J. Pine, Phys. Rev. Lett. 79 (1997) 2359.
[23] T. Shikata, H. Hirata, T. Kotaka, Langmuir 4 (1988) 354.